Electronic Supplementary Material (ESI) for Journal of Materials Chemistry A.

Epitaxial Growth of $ZnWO_4$ Hole-Storage Nanolayers on ZnO Photoanodes for Efficient Solar Water Splitting

Shurong Fu[a,b], Hongyan Hu [a,*], Chenchen Feng[a,b], Yajun Zhang [a], Yingpu Bi[a,*]

[a] State Key Laboratory for Oxo Synthesis & Selective Oxidation, National Engineering Research Center for Fine Petrochemical Intermediates, Lanzhou Institute of Chemical Physics, CAS, Lanzhou, Gansu 730000, China.

*E-mail: yingpubi@licp.cas.cn

[b] University of Chinese Academy of Sciences, Beijing 100049, China.

Experimental Section

All reagents were used without any further purification.

Preparation of ZnO nanorod arrays thin films: The ZnO nanorod arrays were fabricated by the sol-gel spin coating and hydrothermal methods in our previous report[1]. Fluorine-doped tin oxide (FTO, 1.0×5.0 cm^2)-coated glass substrate were ultrasonically cleaned for 20 min with acetone, isopropanol, ethanol and deionized water, respectively. In a typical experimental procedure, 0.05 M zinc acetate dehydrate [$Zn(CH_3COO)_2\cdot 2H_2O$] was dissolved in ethylene glycol monomethyl ether (EM) and stirred at 60 °C for 30 min. Then, an equal amount of diethanolamine (DEA) was added to the mixture to stabilize the solution and stirred at 60 °C for 2 hours. After that, the as-prepared sol was sealed and put for 2 days. Next, the precursor sol (100 μL) was spin coated over an FTO substrate using a vacuum spin coater. The sample was dried in an oven at 150 °C for 15 min and repeated the process for three times. The thin film was annealed in a muffle furnace in air at 350 °C for 30 min to remove residual solvent and obtain the ZnO seed layer. Then, the ZnO seed layer was subjected to the hydrothermal process for the growth of ZnO nanorod arrays. The coated ZnO seed substrate was immersed into the solution mixture to grow ZnO nanorod arrays at 95 °C for 6 h, which contained 0.04 M aqueous solutions of zinc nitrate [$Zn(NO_3)_2\cdot 6H_2O$] and 0.04 M hexamethylene tetraamine (HMT). Finally, the film was washed with deionized water and absolute ethyl alcohol for several times to remove excess HMT and unreacted or non-adherent particles, followed by a drying step in an oven at 60 °C. Then, the ZnO nanorod arrays thin film was annealed in a muffle furnace in air at 250 °C for 1 h with a heating rate of 2 °C min^{-1}.

Preparation of the umbrella array structure of $ZnWO_4$/ZnO**:** The umbrella array structure of $ZnWO_4$/ZnO was fabricated by hydrothermal method. The as-prepared ZnO nanorod array was immersed into the solution mixture to grow umbrella structure of $ZnWO_4$ at 160 °C for 1 h, which contained 0.25 mM aqueous solutions of zinc acetate dihydrate [$Zn(CH_3COO)_2\cdot 2H_2O$] and 0.25 mM sodium tungstate dihydrate ($Na_2WO_4\cdot 2H_2O$). The films were then rinsed thoroughly with deionized water and dried at 60 °C in vacuum. The umbrella array structure of $ZnWO_4$/ZnO as prepared was further annealed in air at 400 °C for 1 h.

Preparation of the umbrella array structure of NiOOH/$ZnWO_4$/ZnO**:** The umbrella array structure of NiOOH/$ZnWO_4$/ZnO was prepared by solution impregnation. The $ZnWO_4$/ZnO thin film was immersed in a mixed solution of 0.5 mM ethylenediamine tetraacetic acid disodium salt (EDTA) and 0.5 mM nickel sulfate hexahydrate ($NiSO_4 \cdot 6H_2O$) for 30 min and then washed with deionized water and dried at room temperature.

***Preparation of the umbrella array structure of FeOOH/ZnWO$_4$/ZnO*:** The umbrella array structure of FeOOH/$ZnWO_4$/ZnO was prepared by solution impregnation. The $ZnWO_4$/ZnO thin film was immersed in a mixed solution of 0.5 mM ethylenediamine tetraacetic acid disodium salt (EDTA) and 0.5 mM ferrous sulfate heptahydrate ($FeSO_4 \cdot 7H_2O$) for 30 min and then washed with deionized water and dried at room temperature.

***Characterization*:** The crystal structures of the films were determined by X-ray diffraction (PANalytical X'Pert PRO) using graphite monochromized Cu Kα radiation (40 kV). The morphology and elemental distributions of these as-prepared products were observed by using a filed-emission scanning electron microscope (JSM-6701F, JEOL, 5kV) with an energy dispersive spectrometer (EDS). The element composition was carried out by using X-ray photoelectron spectroscope (XPS, ESCALAB 250Xi) with X-ray monochromatisation as the excitation source. The UV-vis absorption spectra were recorded on a UV-2550 (Shimadzu) spectrophotometer by using $BaSO_4$ as the reference.

***Photoelectrochemical Measurements*:** The photoelectrochemical measurement of the photoanodes were carried out in a three-electrode configuration (photoanode as working electrode, SCE as reference electrode and Pt as counter electrode) under an air mass 1.5 (AM 1.5G, 100 $mW \cdot cm^{-2}$) illumination provided by a solar simulator. An aqueous solution of 0.02 M KOH was used as the electrolyte and the data was recorded by an electrochemical workstation (CHI760E). The scan rate of linear sweep voltammograms (LSV) was 10 mV s^{-1} and the scanned range was -0.7 V to +0.7 V (vs. SCE). The recorded potentials vs. SCE were converted to the reversible hydrogen electrode (RHE) scale according to the following equation 1: $E_{RHE}=E_{SCE}+0.059pH+E^0_{SCE}$, where E_{SCE} was the experimentally measured potential and $E^0_{SCE}=0.24$ V at room temperature. Stability measurements (current-time) were conducted at a bias voltage of 1.23 V (vs. RHE). Electrochemical impedance spectroscopy (EIS) measurements were performed by applying -0.1 V (vs. SCE) at a frequency range of 10^{-2} Hz to 10^5 Hz with small AC amplitude of 10 mV. The incident photon to current efficiency (IPCE) was measured with the aid of a monochromator (Oriel Cornerstone1301/8 m), and calculated using the following

Equation 2:

$$\mathrm{IPCE}(\%) = \frac{1240 \times \mathrm{I}(\mathrm{mA}/\mathrm{cm}^2)}{\mathrm{P}_{\mathrm{light}}(\mathrm{mW}/\mathrm{cm}^2) \times \lambda(\mathrm{nm})} \times 100 \qquad (2)$$

where I is the measured photocurrent density at a specific wavelength, λ is the wavelength of incident light and $\mathrm{P}_{\mathrm{light}}$ is the measured light power density at that wavelength. Supposing 100% Faradaic efficiency, the maximum applied bias photon to current efficiency (ABPE) was calculated using the following Equation 3:

$$\mathrm{ABPE}(\%) = \frac{\mathrm{I}(\mathrm{mA}/\mathrm{cm}^2) \times (1.23 - \mathrm{V}_{\mathrm{bias}})(\mathrm{V})}{\mathrm{P}_{\mathrm{light}}(\mathrm{mW}/\mathrm{cm}^2)} \times 100 \qquad (3)$$

where I is the measured photocurrent density, $\mathrm{V}_{\mathrm{bias}}$ is the applied potential, $\mathrm{P}_{\mathrm{light}}$ is the incident illumination power density (100 mW·cm^{-2}). The η_{surf} can be calculated by the Equation 4:

$$\eta_{\mathrm{surf}} = \mathrm{J}_{\mathrm{H}_2O}/\mathrm{J}_{\mathrm{Na}_2\mathrm{SO}_3} \qquad (4)$$

Where J_{H_2O} and $J_{Na_2SO_3}$ are the photocurrent density at 0.02 M KOH with/without Na_2SO_3 electrolyte.

Using Ar as a carrier gas, the evolved amounts of H_2 and O_2 from the PEC cell system were analyzed by an online gas analysis system (Labsolar 6A, Beijing Perfectlight Technology Co. Ltd.) and a gas chromatograph (GC 7890A, Agilent Technologies). Light source and electrolyte were the same as these used for above PEC measurements. The produce of H_2 and O_2 was performed in a three-electrode system at a constant bias of 1.23 V_{RHE} under AM 1.5G illumination (100 mW cm^{-2}).

Additional Figures and Discussions

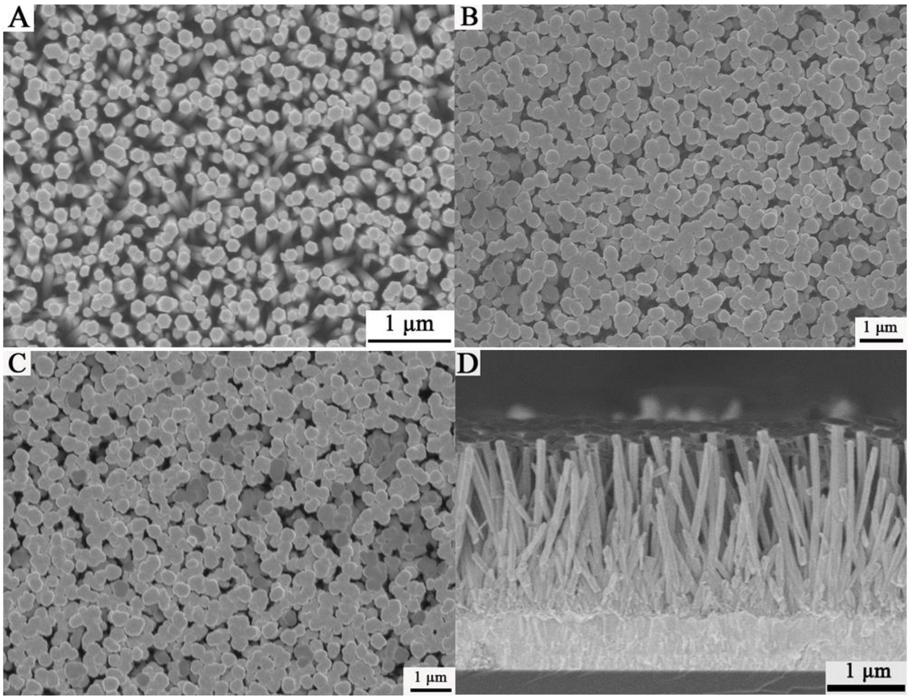

Fig. S1 (A, C) Top-view SEM images of pure ZnO nanorod arrays and umbrella array NiOOH/$ZnWO_4$/ZnO; (B, D) Top-view and cross-section SEM images of $ZnWO_4$/ZnO.

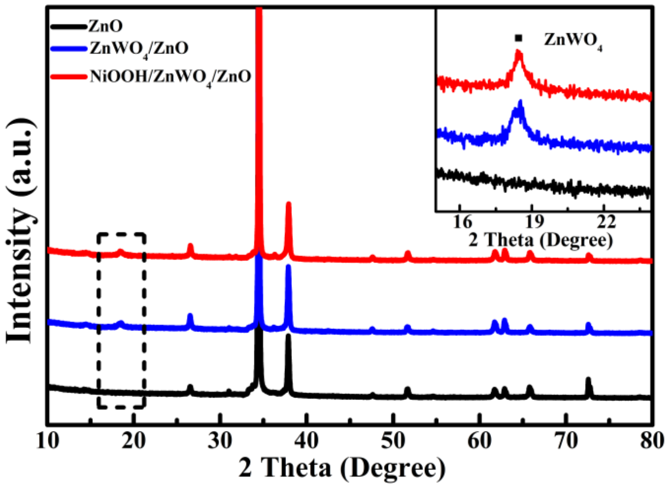

Fig. S2 XRD patterns of pure ZnO nanorod arrays, $ZnWO_4$/ZnO and NiOOH/$ZnWO_4$/ZnO photoanode.

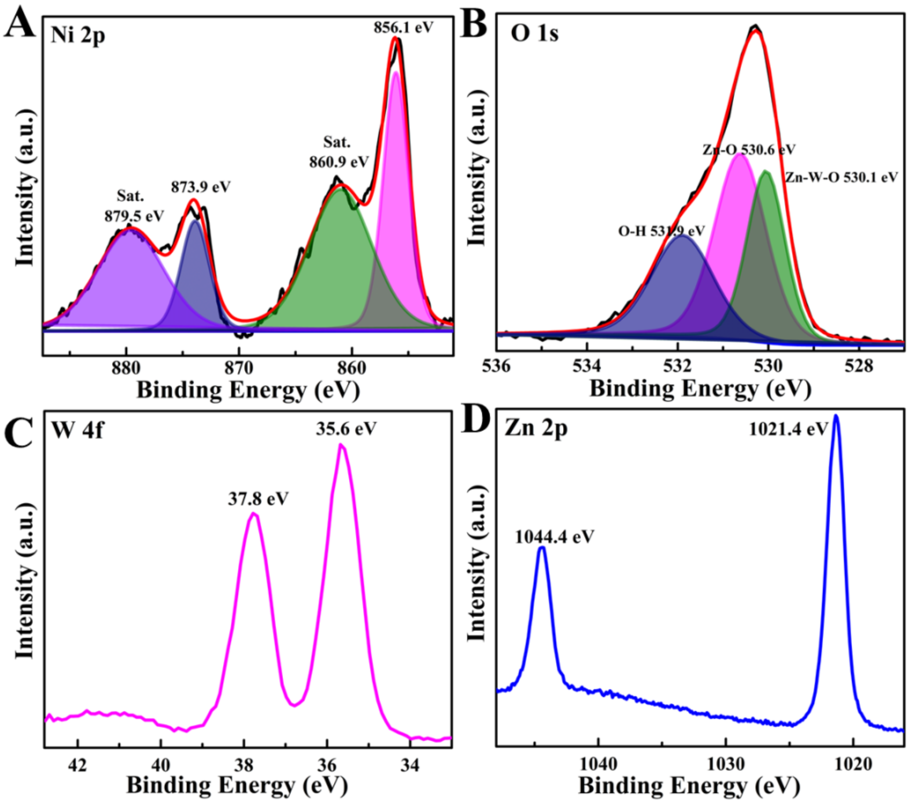

Fig. S3 High-resolution XPS spectra of (A) Ni 2p, (B) O 1s, (C) W 4f and (D) Zn 2p of the NiOOH/$ZnWO_4$/ZnO photoanode.

Additional discussions

Fig. S3 shows the high-resolution Ni 2p, O 1s, W 4f and Zn 2p spectra of NiOOH/$ZnWO_4$/ZnO photoanode. The high resolution O 1s spectra (Fig. S3B) show three peaks at 531.9 eV, 530.6 eV and 530.1 eV, which could be assigned to the chemisorbed hydroxyl oxygen and lattice oxygen of ZnO and $ZnWO_4$, respectively[1, 2]. In Fig. S3C, the high resolution W 4f spectra show two peaks located at 37.8 eV and 35.6 eV, corresponding to W $4f_{5/2}$ and W $4f_{7/2}$, respectively[3]. For the Zn 2p spectra (Fig. S3D), the two peaks of Zn 2p located at 1044.4 eV and 1021.4 eV could be indexed to Zn $2p_{1/2}$ and Zn $2p_{3/2}$, respectively, illustrating that the valence state of zinc species was in the form of Zn^{2+} ions[4].

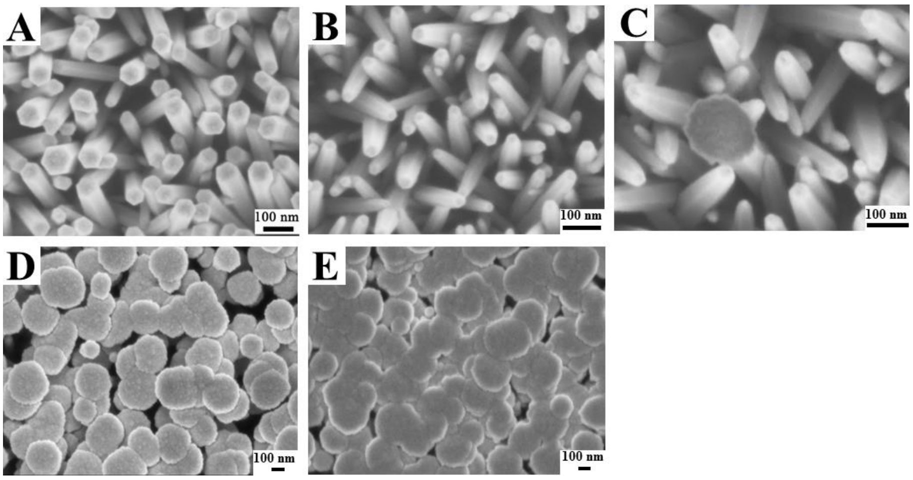

Fig. S4 SEM images of pure ZnO (A), and $ZnWO_4$/ZnO hydrothermal time for 30 min (B), 40 min (C), 90 min (D) and 120 min (E) at 160 °C.

Additional discussions

To reveal the apparent the growth process of $ZnWO_4$ nanoplates on the ZnO nanorod arrays, the hydrothermal reaction time for the ZnO nanorod arrays in Fig. S4 were controlled for 4 hours. The effect of hydrothermal time on the morphology of $ZnWO_4$ was investigated at 160 °C. When the reaction time is 30 min, the top regions of well-defined hexagonal ZnO nanorods have been slightly dissolved into conical structures. The small $ZnWO_4$ nanoplates are formed on ZnO nanorod arrays with the hydrothermal time increased up to 40 min. The umbrella array structure is completely formed with increasing time from 90 min to 120 min. However, when the hydrothermal time is too long, the umbrella array structure of $ZnWO_4$/ZnO is too tight and large in diameter. Therefore, the optimum hydrothermal time is 60 min in this study.

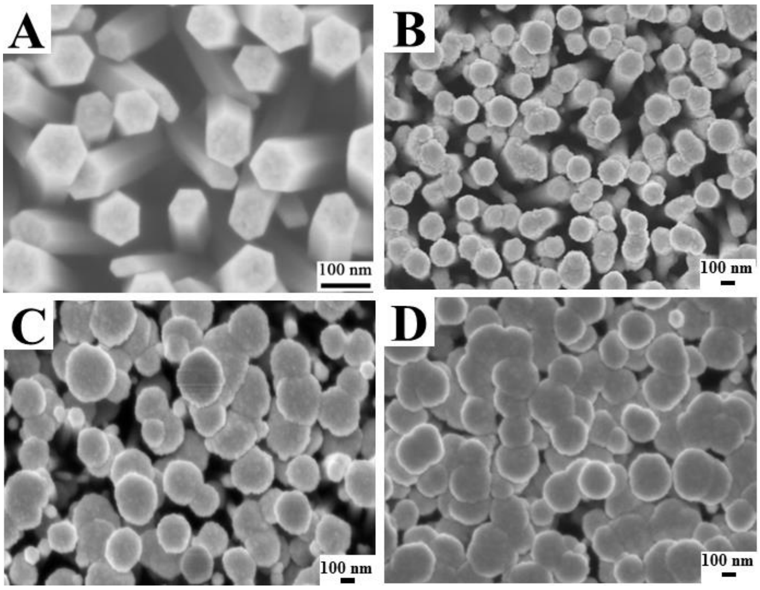

Fig. S5 SEM images of pure ZnO (A) and $ZnWO_4/ZnO$ synthesized at 100 °C (B), 140 °C (C) and 180 °C (D).

Additional discussions

The comparison experiments were designed to elucidate the effect of hydrothermal temperature on the morphology variety of as-prepared $ZnWO_4/ZnO$. As shown in Fig. S5B, C, and D, when the hydrothermal temperature increased from 100 °C to 180°C, the morphology of $ZnWO_4$ changes from particles to umbrella array structure. The umbrella array structure of $ZnWO_4/ZnO$ synthesized at 140 °C is incomplete. However, the umbrella array structure of $ZnWO_4/ZnO$ is too tight and large in diameter with the hydrothermal temperature further increased up to 180 °C, which is harmful for the absorption of light. Therefore, the optimum hydrothermal temperature is 160 °C in this study.

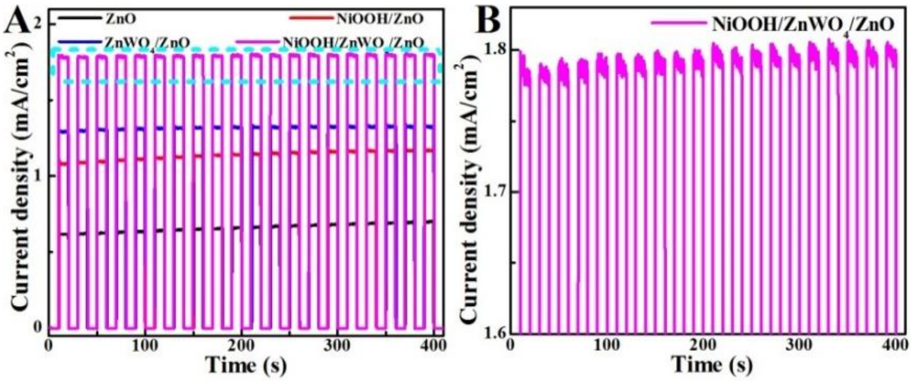

Fig. S6 Amperometric i-t curves of different photoanodes at 1.23 V_{RHE} in 0.02 M KOH (pH=12.3) under AM 1.5 G (100 mW cm^{-2}) illumination, (B) the enlarged view of *i-t* curve for $NiOOH/ZnWO_4/ZnO$.

Additional discussions

Transient photocurrent density *versus* time was recorded at a fixed potential of 1.23 V_{RHE} under light on/off illumination cycles to investigate the photoresponse of different photoanodes. As shown in Fig. S6A, the rise and fall of the photocurrent corresponded well to the illumination being switched on and off. The $ZnWO_4/ZnO$ photoelectrode exhibited higher photocurrent conversion efficiency than pristine ZnO photoanode, indicating that $ZnWO_4$ could enhance the electron-hole separation and transport for improving the photocurrent density of ZnO nanorod arrays. After the modification NiOOH cocatalyst on $ZnWO_4/ZnO$, the photocurrent density could be further enhanced, demonstrating that NiOOH accelerated the water oxidation and decreased the charge transfer resistance at the electrode-electrolyte interface. Additionally, Fig. S6B shows the enlarged *i-t* curve of $NiOOH/ZnWO_4/ZnO$ photoanode, and a slightly transient photocurrent could be observed. However, owing to the rapid hole transfer between $ZnWO_4/ZnO$ interfaces resulted from their well-matched lattices, the transient photocurrent of this photoanode is not obvious.

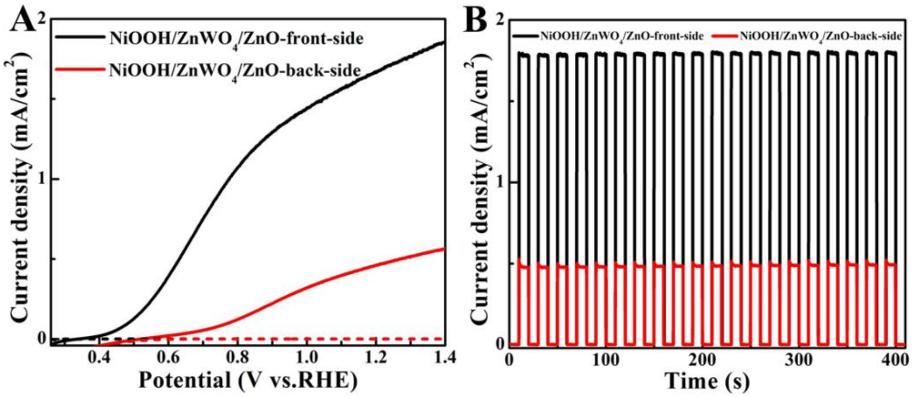

Fig. S7 (A) *J-V* curves in the dark and under AM 1.5G irradiation and (B) i-t curves of NiOOH/$ZnWO_4$/ZnO for front-side illumination and back-side illumination.

Additional discussions

The PEC performances under front-side illumination (ZnO side) and back-side illumination (glass side) have been compared in Fig. S7. It can be clearly observed that compared with front-side illumination, the photocurrent density under back-side illumination has been significantly decreased. Furthermore, owing to the limitations of light penetration-depth in photoelectrode layers, the front-side and back-side illumination would result in different charge transport modes. More specifically, the front-side illumination would induce the electron transport across the entire photoelectrode layers to the FTO fundus. In contrast, the back-side illumination would induce the hole transport across the photoelectrode layers to the electrode/electrolyte interfaces.[5,6] Thereby, it was considered that the hole transport is much more sluggish than electron transport in the present photoanodes, which resulted in higher PEC activities under front-side illumination than that of back-side illumination.

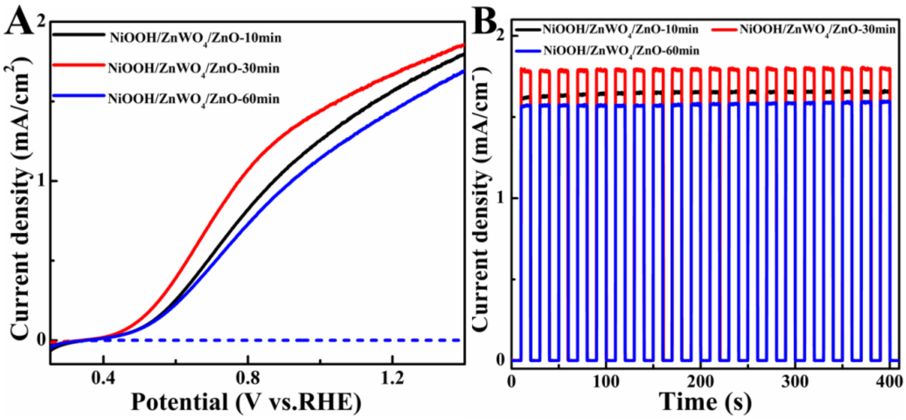

Fig. S8 (A) *J-V* curves and (B) i-t curves for NiOOH/$ZnWO_4$/ZnO photoanodes with different NiOOH impregnation times (from 10 min to 60 min) measured with 0.02 M KOH electrolyte in the dark and under AM 1.5G irradiation

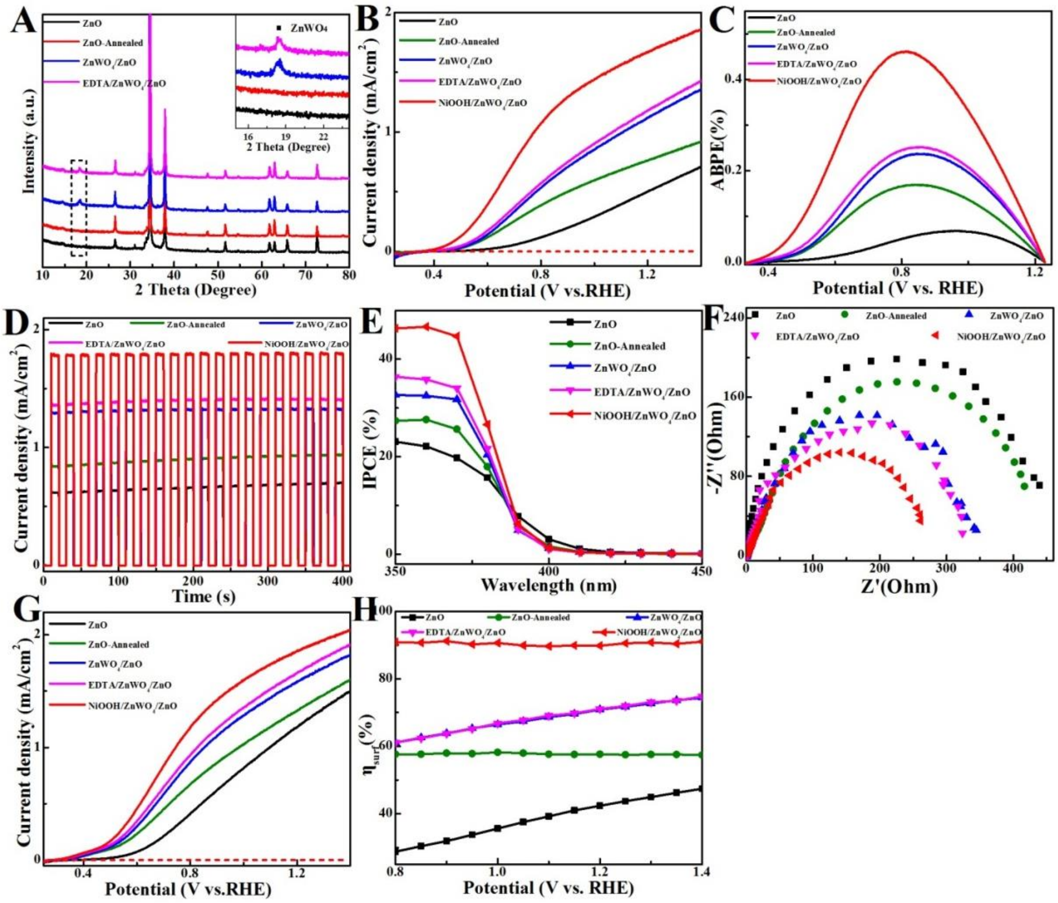

Fig. S9 (A) XRD patterns, (B) *J-V* curves in the dark and under AM 1.5G irradiation, (C) ABPE, (D) i-t curves, (E) IPCE at 1.23 V_{RHE} under monochromatic irradiation, (F) EIS, (G) *J-V* curves with Na_2SO_3 in the electrolyte and (H) η_{surf} for ZnO, ZnO-Annealed, $ZnWO_4$/ZnO, EDTA/$ZnWO_4$/ZnO and NiOOH/$ZnWO_4$/ZnO photoanodes. ZnO-Annealed refer to ZnO anneal at 400 °C.

Additional discussions

Since the synthesis of $ZnWO_4$ and NiOOH with an annealing process and adding into EDTA, respectively, we explored the performance of pure ZnO annealed at 400 °C for 1 h marked as ZnO-Annealed and the performance of EDTA/$ZnWO_4$/ZnO. The XRD patterns of ZnO-Annealed and EDTA/$ZnWO_4$/ZnO are explored shown in Fig. S9A. The results indicated that the crystalline structure of ZnO nanorod arrays and $ZnWO_4$ were not changed after annealed or added into EDTA. Furthermore, the PEC performance of different photoanodes are examined in 0.02 M KOH (pH=12.3) under AM 1.5G simulated sunlight (100 mW cm^{-2}) (Fig. S9). The photocurrent density of the ZnO-Annealed was slightly enhanced to 0.79 mA cm^{-2} at 1.23 V_{RHE} compared to the pristine ZnO nanorod arrays (0.53 mA cm^{-2} at 1.23 V_{RHE}), which may result from the improved crystallinity of ZnO thin films. Additionally, the photocurrent density of EDTA/$ZnWO_4$/ZnO (1.22

mA cm^{-2} at 1.23 V$_{RHE}$) is only a little improvement compared to $ZnWO_4$/ZnO (1.16 mA cm^{-2} at 1.23 V$_{RHE}$) photoanode, which implied that the effect of EDTA on photocurrent is negligible. Transient photocurrent density *versus* time curves, ABPE curves, IPCE curves, EIS curves and the surface charge separation efficiencies (η_{surf}) present the similar results. Therefore, the effect of the annealing process and adding into EDTA on the PEC performances of $ZnWO_4$/ZnO and NiOOH/$ZnWO_4$/ZnO can be excluded.

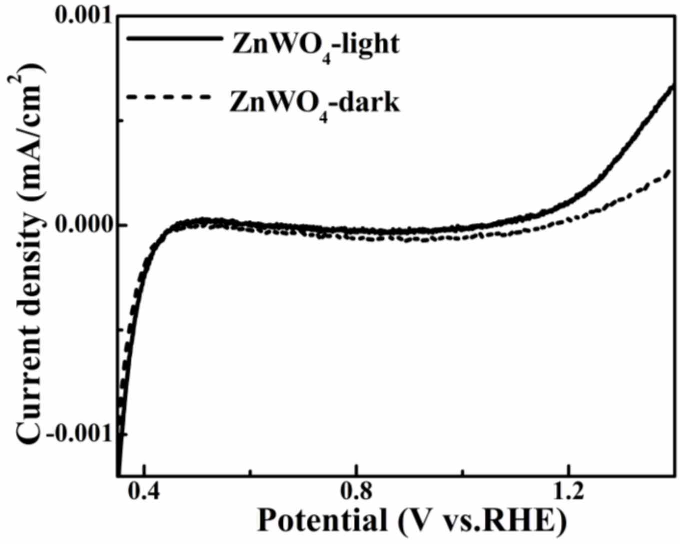

Fig. S10 *J-V* curves of pristine $ZnWO_4$ measured with 0.02 M KOH electrolyte in the dark and under AM 1.5G irradiation (100 mW cm^{-2}).

Additional discussions

As shown in Fig. S10, the photocurrent density of pure $ZnWO_4$ is 1.68 × 10^{-4} mA cm^{-2} at 1.23 V$_{RHE}$, which is almost negligible relative to ZnO (0.53 mA cm^{-2} at 1.23 V$_{RHE}$).

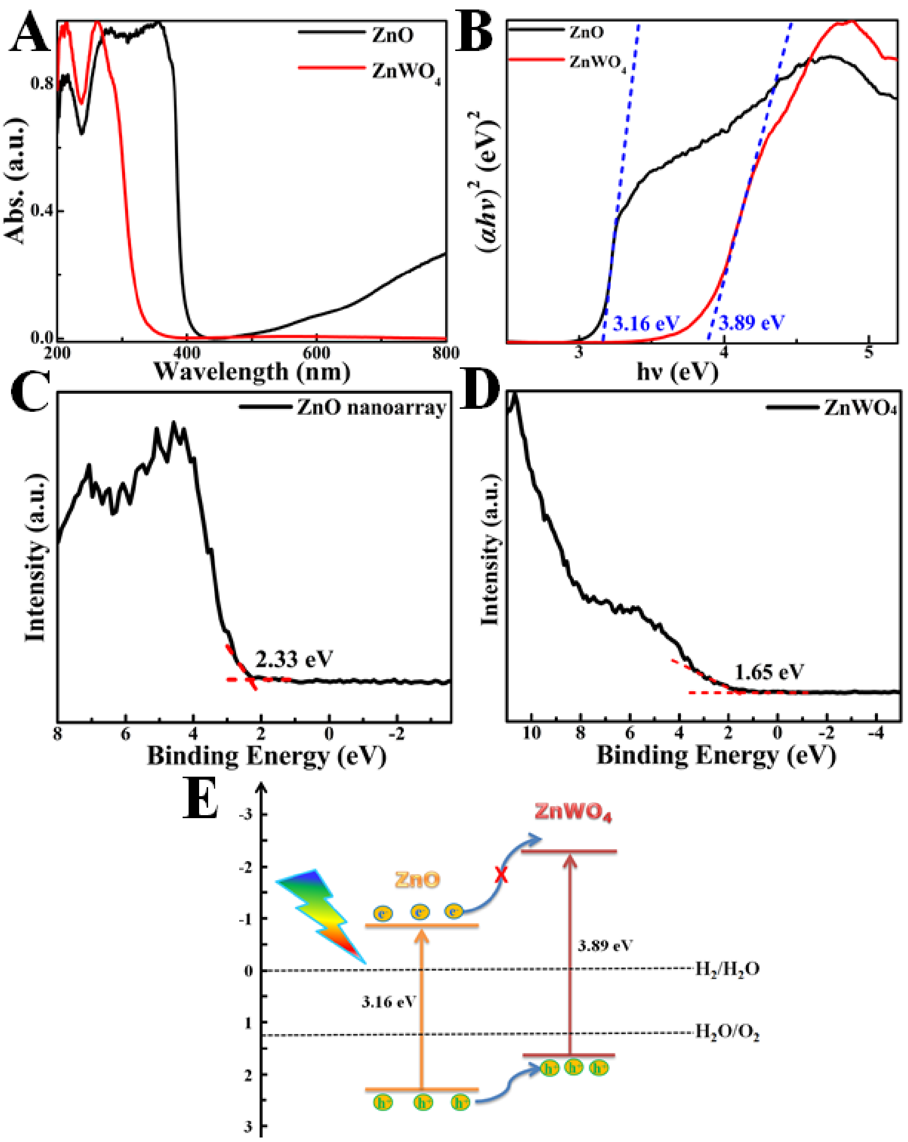

Fig. S11 (A) UV-vis diffuse reflectance spectra and (B) the $(\alpha h\nu)^2$ versus photon energy plots for pristine ZnO and $ZnWO_4$, respectively; (C, D) valence band XPS spectra of pristine ZnO and $ZnWO_4$; (E) schematic band structures of pristine ZnO and $ZnWO_4$.

Additional discussions

The UV-vis diffuse reflectance spectra (DRS) of pristine ZnO nanorod arrays and $ZnWO_4$ are shown in Fig. S11A. The pristine ZnO and $ZnWO_4$ exhibited a characteristic absorption peak near 390 nm and 320 nm, which agreed well with the band gap of 3.16 eV and 3.89 eV (Fig. S11B). The relative valence band (VB) XPS of pristine ZnO and $ZnWO_4$ are 2.33 eV and 1.65 eV (Fig. S11C and D). Therefore, the conduction band (CB) of pristine ZnO and $ZnWO_4$ would occur at -0.83 eV and -2.24 eV, respectively. Based on the above results, the schematic band structures of pristine ZnO and $ZnWO_4$ is shown in Fig. S11E. As a result of the wide bandgap (E_g=3.89 eV) of

$ZnWO_4$, it almost cannot be excited under AM 1.5G simulated sunlight (100 mW cm^{-2}). Therefore, under illumination, plenty of the photogenerated electrons and holes are formed on the conduction band and valance band of ZnO, respectively. The position of VB for ZnO is more positive than that of $ZnWO_4$, thus the photogenerated holes could transfer easily from ZnO into the VB of $ZnWO_4$. However, the photogenerated electrons are blocked from the CB of ZnO to $ZnWO_4$, due to the position of CB for $ZnWO_4$ is more negative than that of ZnO. Furthermore, the valence band position of $ZnWO_4$ vs NHE could be calculated according to the following equation[7]:

$$E_{NHE} = E_{work\ function} + E_{Fermi\ level} - 4.44$$

The work function of $ZnWO_4$ is 4.8 eV,[8,9] and the valence band position of $ZnWO_4$ (vs NHE) is equal to 2.01 eV, which is consistent with the previous reports.[10,11] Moreover, the work function of ZnO is 5.3 eV[12], and the calculated valence band position of ZnO (vs NHE) is 3.19 eV. Therefore, relative to NHE reference, the valence band of $ZnWO_4$ is also matched to that of ZnO.

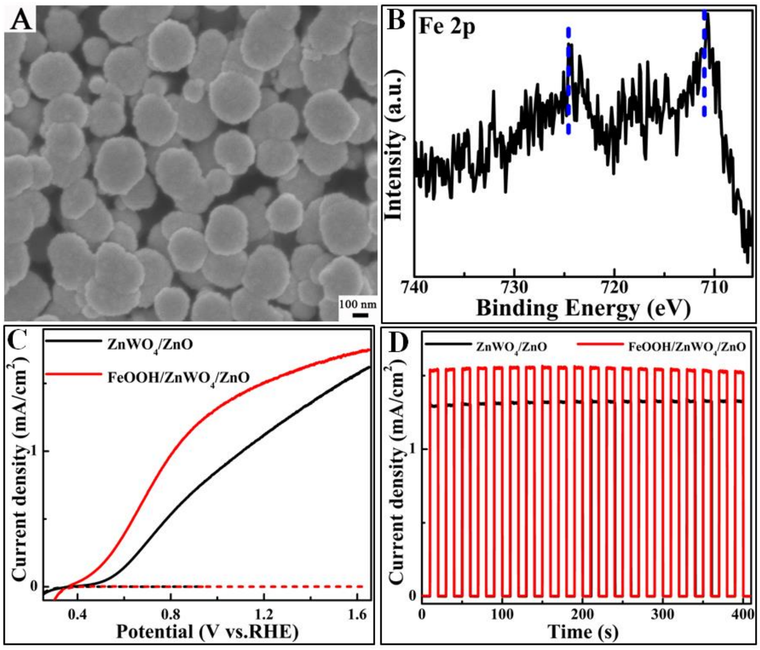

Fig. S12 (A) Top-view SEM images and (B) high-resolution XPS spectra of Fe 2p for $FeOOH/ZnWO_4/ZnO$; (C) *J-V* curves in the dark and under AM 1.5G irradiation and (D) i-t curves for $ZnWO_4/ZnO$ and $FeOOH/ZnWO_4/ZnO$ photoanodes.

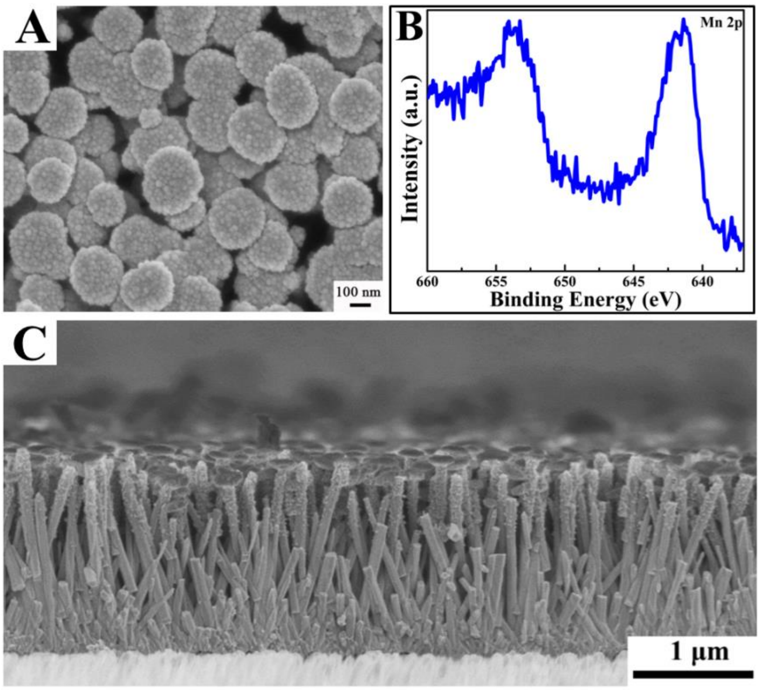

Fig. S13 (A, C) Top-view and cross-sectional view SEM images and (B) high-resolution XPS spectra of Mn 2p for $MnO_2/ZnWO_4/ZnO$.

Additional discussions

In order to further illustrate the existence of hole on the surface of $ZnWO_4$, the oxidation cocatalyst MnO_2 was selectively deposited on $ZnWO_4$ by photo-deposition method[13]. As shown in Fig. S13A and C, it can be clearly observed that MnO_2 nanoparticles have been uniformly dispersed on the surface. Furthermore, the high resolution spectrum for Mn 2p peaks located at 653.5 eV and 641.7 eV clearly confirmed the formation of MnO_2 nanoparticles (Fig. S13B). This result indicates that $ZnWO_4$ could serve as a hole-storage layer for promote the hole transfer from ZnO nanowires arrays for selective oxidation of $MnSO_4$ into MnO_2 by the photo-deposition method.

Notes and references

1. S. Fu, B. Zhang, H. Hu, Y. Zhang and Y. Bi, *Catal. Sci. Technol.*, 2018, **8**, 2789-2793.

2. Y. Wang, L. Liping and G. Li, *Appl. Surf. Sci.*, 2017, **393**, 159-167.

3. L. Sun, X. Zhao, C.-J. Jia, Y. Zhou, X. Cheng, P. Li, L. Liu and W. Fan, *J. Mater. Chem.*, 2012, **22**, 23428-23438.

4. K. Yuan, Q. Cao, X. Li, H. Y. Chen, Y. Deng, Y. Y. Wang, W. Luo, H. L. Lu and D. W. Zhang, *Nano Energy*, 2017, **41**, 543-551.

5. Y. Liang, T. Tsubota, L. P. A. Mooij and R. van de Krol, *J. Phys. Chem. C,* 2011, **115**, 17594-17598.

6. L. Zhang, E. Reisner and J. J. Baumberg, *Energy Environ. Sci.*, 2014, **7**, 1402-1408.

7. H. Yu, R. Shi, Y. Zhao, T. Bian, Y. Zhao, C. Zhou, G. I. N. Waterhouse, L. Z. Wu, C. H. Tung and T. Zhang, *Adv. Mater.*, 2017, **29**, 1605148.

8. P. Li, X. Zhao, C. j. Jia, H. Sun, L. Sun, X. Cheng, L. Liu and W. Fan, *J. Mater. Chem. A*, 2013, **1**, 3421-3429.

9. C. Zhang, H. Zhang, K. Zhang, X. Li, Q. Leng and C. Hu, *ACS Appl. Mater. Interfaces*, 2014, **6**, 14423-14432.

10. Y. Huang, Y. Gao, Q. Zhang, J. j. Cao, R. j. Huang, W. Ho and S. C. Lee, *Appl. Catal. A: Gen.*, 2016, **515**, 170-178.

11. D. W. Kim, I. S. Cho, S. S. Shin, S. Lee, T. H. Noh, D. H. Kim, H. S. Jung and K. S. Hong, *J. Solid State Chem.*, 2011, **184**, 2103-2107.

12. C. J. Lee, T. J. Lee, S. C. Lyu, Y. Zhang, H. Ruh and H. J. Lee, *Appl. Phys. Lett.*, 2002, **81**, 3648-3650.

13. R. Li, F. Zhang, D. Wang, J. Yang, M. Li, J. Zhu, X. Zhou, H. Han and C. Li, *Nat. Commun.*, 2013, **4**, 1432.